ELSEVIER

Biophysical Chemistry 60 (1996) 119–133

Biophysical Chemistry

The conformation of xanthene dyes in the myosin sulfhydryl one binding site
Part I. Methods and model systems

Thomas P. Burghardt *, Katalin Ajtai

Department of Biochemistry and Molecular Biology, Mayo Foundation, Rochester, MN 55905, USA

Received 14 August 1995; revised 4 January 1996; accepted 10 January 1996

Abstract

Derivatives of the fluorescent probes fluorescein and rhodamine specifically and covalently modify the highly reactive thiol (SH1) of myosin subfragment 1 (S1). Both probes develop circular dichroism (CD) upon modification of SH1 at the visible absorption band of the chromophore. A model system of chiral complexing agents (aromatic chiral amines) interacting with fluorescein in solvent develops a CD signal that mimics that produced by S1. The model system suggests that a specific interaction of the probe with an aromatic chiral residue in the SH1 binding pocket induces the CD signal. Several other spectroscopic signals, including absorption and fluorescence intensity and anisotropy, characterize the fluorescein or rhodamine binding to SH1. A coupled dipole method is adapted to interpret these spectroscopic signals in terms of the probe–S1 complex conformation. The computation of the orientation of the principal hydrodynamic frame (PHF) of S1 from its crystallographic α-carbon backbone structure permits the known orientation of the probe in the PHF of S1 to further constrain the conformation of the probe–S1 complex. The coupled dipole interpretation of spectroscopic data combined with constraints relating the probe dipole orientation to the PHF of S1 determines the conformation of the probe–S1 complex. The methods developed here are applied to the spectroscopic signals from fluorescein or rhodamine in the SH1 binding site of S1 to obtain an atomic resolution model of the probe–S1 conformation [Ajtai and Burghardt, Biochemistry, 34 (1995) 15943–15952].

Keywords: Myosin; Tryptophan; Rhodamine dimer; Fluorescein; Chiral complexing agent; Circular dichroism; Coupled dipoles

1. Introduction

Xanthene probes of the highly reactive sulfhydryl, SH1, on the myosin cross-bridge or subfragment 1 (S1) followed the dynamics of cross-bridge movement during the active cycle. These probes efficiently fluoresce visible light following excitation and report their orientation by techniques including fluctuations in fluorescence polarization [1], steady-state linear dichroism [2], and time-resolved polarized fluorescence photobleaching recovery [3]. The probe specificity and rigidity in the SH1 binding pocket permitted data interpretation in terms of the cross-bridge, rather than the probe, dynamics. A multiple probe approach, utilizing several specific probes of SH1 with transition dipole moments vari-

* Corresponding author. E-mail: burghardt@mayo.edu.

PII S0301-4622(96)00014-2

ously oriented on S1, allowed a more sophisticated level of data interpretation in terms of cross-bridge rotational movement about the axes of its principal hydrodynamic frame (PHF). From the latter work we created an animated model of the angular trajectory of cross-bridge movement during contraction [4,5]. We now begin to develop the spectroscopic methods to surmise an atomic resolution structure of the probe–S1 conformation. Ultimately, our wish is to interpret spectroscopic probe data in terms of local structural changes in S1 during ATP hydrolysis.

The crystallographic structure of the myosin S1 α-carbons provides the framework for investigating the conformation of the probe–S1 interaction at SH1 [6]. Our approach is to observe several spectroscopic parameters from the uncomplexed probe, the S1 alone, and the probe–S1 complex, and then to account for the difference between the isolated and complexed molecular spectroscopic parameters by coupling the dipole oscillators of the probe with the side chains within the SH1 binding pocket [7,8]. The strength of the coupled dipole interaction depends on the distance and orientation of the probe relative to the S1 side chains thereby relating spectroscopic parameters to probe–S1 conformation. This approach, in various representations, was used successfully to study the conformation of other covalent and noncovalent dye–protein systems such as bilirubin–albumin [9], dye–enzyme complexes [10–13], and the fluorescein–immunoglobulin system [14–16]. In concept this work is not essentially different from other tertiary structural investigations of S1 based on spectroscopic parameters [17–27] except that the resolution is higher. The atomic level resolution is feasible because the crystallographic S1 structure eliminates structurally impossible but spectroscopically equivalent probe–S1 conformations.

We present our work in two reports. This paper, Part I, deals with certain theoretical methods and simple model systems while Part II [28] reports our findings on the probe–S1 conformation. Specifically, in Part I we summarize, and adapt for application to S1, methods for modeling spectroscopic data in terms of molecular conformation. We work with the spectroscopic signals of absorption, circular dichroism (CD), and, fluorescence intensity and anisotropy from aromatic molecules and their complexes. We deal with the implications of these signals concerning: (i) the local interactions of the probe with a chiral aromatic side chain in the SH1 binding pocket, and, (ii) the orientation of the probe relative to the PHF of S1. One of the dye molecules studied, rhodamine, has a stoichiometry of two probes per S1 and a spectroscopic signature characteristic of a bound dimer [29]. Consequently, we handle the three-molecule problem involving the rhodamine dimer and the aromatic side chain in the binding pocket using a stepwise (approximate) approach. First we solve the conformation of the dimer in solution [30,31] and then treat the dimer as a single molecule interacting with the chiral aromatic side chains in the SH1 binding pocket. The second purpose of this paper is to demonstrate and explain induced chirality in xanthenes using chiral amines [9,10,32]. This is a model for the observed chirality in the fluorescein and rhodamine probes induced by S1.

We apply the formal methods introduced here to deduce the conformation of the fluorescein or rhodamine dyes bound to S1 in Part II. The importance of rhodamine as a probe of the contractile apparatus motivates the efforts needed to address the difficulties of this three-molecule problem. Fluorescein, also a widely used probe of the contractile apparatus, is monomeric when specifically bound to S1 and its conformation in the SH1 binding pocket is also investigated. The greater simplicity of fluorescein–S1 complex, over the three-molecule complex, helps to remove certain ambiguities in the probe–S1 conformation determination.

2. Materials and methods

2.1. Chemicals

Acetonitrile, N,N-dimethylsulfoxide (DMSO), and dimethylformamide (DMF) were from Sigma (St. Louis, MO). Acetone was from Fisher (Pittsburgh, PA), and ethanol (alcohol) from J.T. Baker (Phillipsburg, NJ). The chiral amines (or chiral templates) (*R*)-(+)- or (*S*)-(−)-N,αdimethylbenzylamine ((*R*)-(+)- or (*S*)-(−)-DMBA), (*R*)-(+)- or (*S*)-(−)-N,αmethylbenzylamine ((*R*)-(+)- or (*S*)-(−)-MBA), (*R*)-(+)- or (*S*)-(−)-N,N,αdimethylphenethylamine ((*R*)-(+)- or (*S*)-(−)-DMPA), and (*R*)-(+)- or (*S*)-(−)-butylamine ((*R*)-(+)- or (*S*)-

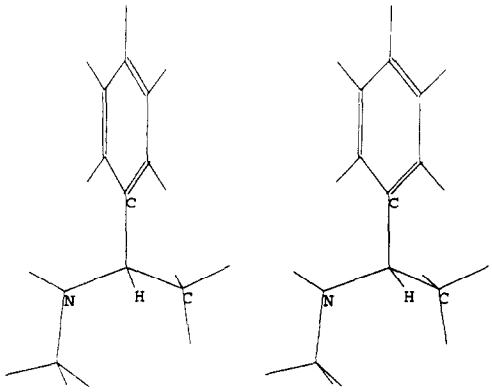

Fig. 1. Uncrossed stereo view of the chiral amine (*R*)-(+)-N, α dimethylbenzylamine looking towards the chiral center from opposite the lowest priority ligand H (i.e., the CH bond on the chiral center projects into the plane of the paper). The (*R*) designation results from the clockwise arrangement of groups surrounding the chiral center from N (the highest priority ligand) to CH_3 (the second to the lowest priority ligand). In the (*S*)-isomer one interchanges the N and CH_3 ligands.

(−)-BA) were from Aldrich (Milwaukee, WI). Fig. 1 shows the (*R*)-(+)-DMBA where the *R* designation comes from the Cahn–Ingold–Prelog (CIP) convention [33–35] and the + sign refers to optical rotation under conditions specified by Aldrich. Sodium fluorescein was from Kodak (Rochester, NY). 5′-iodoacetamidofluorescein (5′IAF) was from Molecular Probes (Eugene, OR). Solvents were HPLC grade and all other chemicals were analytical grade.

2.2. Solutions

The sodium fluorescein was dissolved in DMF then added at 150 μM concentration to 0.5–1.5 M of the chiral amines and 2.5% DMF in acetonitrile. The molar ratio between fluorescein and the chiral complexing agent was between 1:820 and 1:9800. The protein buffer is 50 mM Tris HCl at pH 8 and 0.2 mM PMSF.

2.3. Preparation and labeling of myosin subfragment 1

The preparation of S1 and its labeling with the fluorescent probes 5′IAF and 5′-iodoacetamidotetramethylrhodamine (5′IATR) (5′F-S1 and 5′R-S1) are described in Part II.

2.4. Spectroscopic measurements and data fitting

We measured absorption on a Beckman DU650 (Beckman Instruments, Fullerton, CA) or a Cary 4 (Varian Instruments, Houston, TX) spectrophotometer, and circular dichroism (CD) on a Jasco J-720 spectropolarimeter (Jasco, Tokyo). Spectral resolution was 1 nm. We measured fluorescence on a SLM 8000 spectrofluorometer (SLM Instruments, Urbana, IL). Fluorescence emission spectra were recorded with monochromator slits of 2 nm. All measurements were made in the steady-state at 6°C.

3. Theory

We bring together here a diverse set of analytical tools needed to interpret the various spectroscopic signals from the probe, the S1, the probe–S1 complex, and the probe–S1 complex oriented in a muscle fiber, in terms of constraints on the probe–S1 conformation. We overview the content of 'Theory' to summarize the main features of the methods and to emphasize that they are ultimately related by their implications for a common and practical structural problem. Specifics concerning the analytical methods and the references to the original work are found subsequently.

Section 3.1 deals with the effect of dimer formation on the rhodamine solution absorption spectra. We show how we determined the dimer association constant and separated the extinction coefficients, ϵ_M and ϵ_D, of the monomer and dimer forms. The dipole strengths and energies are computed from ϵ_M and ϵ_D. These quantities are central to the coupled dipole interaction in dimers described in Section 3.2.

Theory Sections 3.2 and 3.3 provide the introduction to coupled dipole theory and a discussion of probe–solvent interactions for one of the xanthene probes. Coupled dipoles describe a particular interaction, among general probe–solvent interactions, applicable to both the dimer and probe–S1 conformation problems. General probe–solvent interactions are discussed in Section 3.3 to justify our use of energy shifts, in some of the probe absorption data,

in the coupled dipole model for the probe–S1 interaction.

Sections 3.4 and 3.5 deal with the transition dipole orientation in chromophores. Section 3.4 is concerned with the transition dipole orientation of uncoupled chromophores. This part is mainly descriptive since many of the dipole moments were measured experimentally from oriented samples and/or calculated by known methods and the values we use are from the literature. Section 3.5 deals with the estimation of the emission dipole orientation from rhodamine dimers. The estimates are based on findings from the coupled dipole theory that provides the positions of the interacting dipoles. By the use of the ideas in Sections 3.4 and 3.5, we fix the dipole orientation within the interacting molecules' atomic coordinates to produce the complex conformation.

Section 3.6 is a discussion of Förster energy transfer and its implications for xanthene probes interacting with aromatic residues in a protein. The energy transfer efficiency from tryptophan to the xanthene probe modifying SH1 provides a simple constraint on the possible contributors to the probe–S1 interaction since we can exclude from consideration tryptophan residues beyond the characteristic energy transfer distance.

Finally, Section 3.7 is a calculation of the PHF of S1 from its α-carbon coordinates. This computation fixes the orientation of the PHF in the atomic coordinates of S1. We previously determined the 5'IATR probe dipole orientation relative to the PHF of S1 from independent hydrodynamic experiments. This data adds another highly restrictive constraint on the probe–S1 conformation.

The ideas in Sections 3.1–3.7 will be combined to constrain the conformation for xanthene probes in the SH1 binding pocket of S1 in Part II. In the following, bold face characters are vectors or vector operators, and operators are single π-electron operators.

3.1. The bimolecular reaction in homodimer formation

Identical molecules in solution may self-associate to form dimers or higher order complexes. Neglecting higher order complexes the self-association follows the reaction scheme,

$$\mathrm{M} + \mathrm{M} \underset{k_2}{\overset{k_1}{\rightleftarrows}} \mathrm{D} \tag{1}$$

where M is the monomer and D the dimer. The equilibrium constant for this reaction, $K = k_1/k_2$, relates the monomer and dimer concentration at equilibrium, [M] and [D], to the initial monomer concentration, $[\mathrm{M}_0]$, such that,

$$[\mathrm{M}] = \left([\mathrm{D}]/K\right)^{1/2} \tag{2}$$

and

$$\frac{2[\mathrm{D}]}{[\mathrm{M}_0]} = 1 + \frac{1 - \left(1 + 8K[\mathrm{M}_0]\right)^{1/2}}{4K[\mathrm{M}_0]} \tag{3}$$

The absorption, $A(\epsilon_\mathrm{M}, \epsilon_\mathrm{D}; K)$, is linear in the extinction coefficients ϵ_M and ϵ_D for pure monomer and dimer, respectively, and nonlinear in K. We measure A as a function of wavelength and at three or more $[\mathrm{M}_0]$'s to obtain a column of absorptions, A_i, such that,

$$A_i = \left\{\epsilon_\mathrm{M}\left([\mathrm{D}]_i/K\right)^{1/2} + \epsilon_\mathrm{D}[\mathrm{D}]_i\right\}\ell_i \tag{4}$$

where subscript i refers to experiments with initial concentration $[\mathrm{M}_0]_i$ and light path ℓ_i. For a particular choice of K and wavelength, the linear parameters in the system of equations represented by Eq. 4 are solved for by a least squares protocol with constraints requiring that ϵ_M and ϵ_D are $\geqslant 0$ [36]. We chose a best K by minimizing the sum of the χ^2's at each wavelength. The best choice for K was used for the equilibrium constant when computing ϵ_M and ϵ_D as a function of wavelength. The generalization of this procedure to the bimolecular reaction in heterodimer formation is outlined in Appendix A.

3.2. The coupled dipole interaction

3.2.1. General

We use dipole–dipole coupling to describe the interaction between aromatic molecules in a complex [7,8,37]. We consider a system of two different molecules with an electronic Hamiltonian given by,

$$\mathrm{H} = \mathrm{H}_0^1 + \mathrm{H}_0^2 + V \tag{5}$$

where H_0^i is the electronic Hamiltonian of the ith isolated molecule and V is the interaction potential. V is the Coulomb interaction for neutral molecules approximated by the first nonvanishing term in the multipole expansion of V, i.e., the dipole–dipole interaction,

$$V(\boldsymbol{\mu}^1, \boldsymbol{\mu}^2) = \frac{\boldsymbol{\mu}^1 \cdot \boldsymbol{\mu}^2 - 3(\boldsymbol{\mu}^1 \cdot \boldsymbol{n})(\boldsymbol{\mu}^2 \cdot \boldsymbol{n})}{(r_{1,2})^3} \qquad (6)$$

where $\boldsymbol{\mu}^i$ is the electric dipole vector operator and $\boldsymbol{r}_{1,2} = \boldsymbol{n} r_{1,2}$ is the vector connecting the dipole moments of the interacting molecules. We assume there is no other interaction between the molecules. The dipole–dipole approximation is inaccurate for molecules separated by distances comparable to the distance of charge separation in the dipole (the dipole moment of the lowest energy transition of fluorescein is equivalent to one electron separated by 1–2 Å). We encounter distances between molecules of 3–4 Å, or about the Van der Waals distance, in the calculations carried out below. Alternatively we could use the point monopole approximation [7,8,38,39]. The point monopoles for the fluorescein and rhodamine–dimer probes are determined with molecular orbital calculations of the excited state charge distributions. The point monopole charges are compared to the experimental through observed dipole moments. The point monopoles for several of the aromatic amino acids were published [40–42]. We did not attempt to use the point dipole approximation because the accuracy of our method is probably limited by other considerations including the assumption that a bimolecular interaction causes all of the perturbations of the probe spectroscopic parameters.

We couple the observable lowest energy excited states of the interacting molecules with the Hamiltonian for the complex given in Eq. 5. It is assumed that the ground state is excluded from interaction with excited states, configurations involving simultaneous excitation of interacting groups are neglected, no charge transfer occurs between interacting groups, and the static dipole of the ground state is neglected. Diagonalization of the Hamiltonian matrix gives the wave functions and consequently the ith excited state transition energy E_i, dipole strength $D_{0,i}$, and rotary strength $R_{0,i}$, for the coupled system [43]. Calculations are compared with experiment using these quantities such that [44],

$$D_{0,i} = 9.18 \times 10^{-3} \int \epsilon \, d\lambda / (\lambda \rho^2 / n) (\text{Debye}^2) \qquad (7)$$

$$R_{0,i} = 0.248 \int \Delta\epsilon \, d\lambda / (\rho \lambda)$$

$$(\text{Debye–Bohr magneton}) \qquad (8)$$

where ϵ is the extinction coefficient, $\Delta\epsilon$ is the CD extinction coefficient, n is the solvent index of refraction, and $\rho = (n^2 + 3)/3$ is the Lorentz correction to the excitation field due to the polarizability of the solvent.

The intrinsic magnetic dipole moment of the xanthene dyes is neglected in all of the calculations. The magnetic and electric dipoles in tryptophan or tyrosine residues of S1 couple to the xanthene electric dipoles in probe labeled S1 to give the induced CD signal in the xanthene absorption bands [41,43–47].

3.2.2. Practical

The dipole–dipole interaction potential depends (nonlinearly) on the distance between the dipoles, $r_{1,2}$. This parameter may be estimated without searching by considering the matrix form of the Hamiltonian from Eq. 5,

$$H\boldsymbol{v} \equiv \left[\mathscr{E} + \mathbb{R}/(r_{1,2})^3\right]\boldsymbol{v} = E\boldsymbol{v} \qquad (9)$$

where $\boldsymbol{v}$ is an eigenvector, $\mathbb{R}$ is the matrix containing the angular dependence of the dipole–dipole interaction, $\mathscr{E}$ is the diagonal matrix containing the energies of the noninteracting molecules, and, E is an eigenvalue corresponding to the energy of the bimolecular complex. Rearranging Eq. 9 and using the identity matrix, $\mathbb{I}$, we may write,

$$(E\mathbb{I} - \mathscr{E})^{-1}\mathbb{R}\boldsymbol{v} = (r_{1,2})^3 \boldsymbol{v} \qquad (10)$$

implying that diagonalization of $(E\mathbb{I} - \mathscr{E})^{-1}\mathbb{R}$ will produce $(r_{1,2})^3$ as an eigenvalue. All possible orientations of the dipole moments are varied to find the best solution in our calculation of the conformation of the interacting molecules. In each trial, $\mathbb{R}$ is computed, E's are estimated using the observed energies of the complex, $\mathscr{E}$'s are estimated from the observed energies of the isolated molecules, and $(E\mathbb{I} - \mathscr{E})^{-1}\mathbb{R}$ is diagonalized to find its eigenvalues.

The diagonalization can be carried out independently for several of the observed E's. Each eigenvalue giving an $r_{1,2}$ that falls within a physically reasonable range is used in subsequent calculations of transition energy, dipole strength, rotary strength, and (see Section 3.4 below) fluorescence anisotropy for comparison with experimental observations.

3.3. The effect of probe–solvent interactions on absorption and emission

The effect of molecular interactions on the spectroscopic properties of a chromophore is the primary concern of this paper. We will propose that a specific interaction between the xanthene probe and a nearby polarizable residue in S1 is the source of the spectroscopic perturbation of the probe when it modifies SH1. The contributions from other spectroscopic perturbants in the system, however, must also be examined. One approach for this examination is in the terms of a general solute–solvent interaction problem where the local environment for the probe near SH1 is one 'solvent'.

The effect of probe–solvent interactions on characteristics of probe absorption and emission was elegantly addressed by Bayliss [48], Marcus [49–52], and McRae [53]. McRae's approach uses a point dipole interaction model and calculates energy shifts in absorption and emission maxima with second order perturbation theory. Marcus' approach is more general, using free energy differences to formulate spectral shifts and broadening without first assuming a model for the interaction. We adopt McRae's treatment for many solvent molecules and one solute molecule. This models our system of a probe (the solute) in the presence of buffer or S1 (the solvent).

The energy shift in the absorption maximum of the solute, due to interaction with the solvent, for the transition from the ground state to the ℓth excited state, is given by,

$$\Delta E_{0\to\ell} = \sum_{j\neq 0} f_{j,0} - \sum_{j\neq\ell} f_{j,\ell} + F(\mu_{00}, \mu_{\ell\ell}, D) \tag{11}$$

where the sum is over eigenstates of the noninteracting system. Terms in f describe dispersive interactions that cause energy shifts referred to as the polarization red shifts [54]. These terms originate from the near instantaneous reaction of the solvent to a change in charge distribution in the solute dipole due to the absorption of a photon.

Terms in F in Eq. 11 depend on the electrostatic properties of the solvent, such as dielectric constant D, and on the permanent dipoles of the solute, μ_{00} and $\mu_{\ell\ell}$. When complete solvent dipole relaxation occurs before photon emission from the solute, as is likely in our application, then the shift in the emission energy due to solvent interaction, $\Delta E_{\ell\to 0}$, is given by,

$$\Delta E_{\ell\to 0} = \sum_{j\neq 0} f_{j,0} - \sum_{j\neq\ell} f_{j,\ell} + F'(\mu_{00}, \mu_{\ell\ell}, D) \tag{12}$$

where $F' \neq F$ from Eq. 11 but F' is a function of the same arguments. The Stokes shift, $E_s \equiv \Delta E_{0\to\ell} - \Delta E_{\ell\to 0} = F - F'$, is independent of the polarization red shift. Stokes shift changes in the presence of different solvents are used to estimate the permanent dipole moments of the solute [55]. We compare E_s from free 5′IAF with 5′F-S1 to examine the difference in the interaction of the solvent with the probe in these systems.

We show in 'Results' that E_s(5′F-S1) ≈ E_s(5′IAF) even as a function of temperature when the rate of solvent relaxation changes. This suggests that the electrostatic and dipole relaxation properties of the solvent near the probe are equal for 5′IAF and 5′F-S1 so that the observed red shift in the absorption maximum of the probe upon binding to S1 is from the altered polarizability of groups near to the probe in 5′F-S1.

The question of whether or not the polarization red shift is correctly modeled by a specific dipole–dipole interaction between the probe and a residue in S1 remains unresolved. We address this issue here and in Part II with several lines of evidence implicating Trp510 as the principal interacting residue. Here we model the hypothetical probe–tryptophan interaction in S1 with the simple system of fluorescein interacting with a chiral amine in solution. We show in 'Results' that the chiral amine–fluorescein interaction mimics the fluorescein–S1 interaction in the absorption and CD changes upon association of the chiral amine with the probe. These results suggest

that the fluorescein–S1 interaction is related to the close association of the probe with a single aromatic side chain in S1.

3.4. Chromophore transition dipole orientation within the molecular structure

The theory of interacting dipoles summarized in Section 3.2 provides a means for determining the relative orientation of the interacting transition dipoles. We relate dipole orientation to the atomic structure of the chromophore to estimate the relationship of the interacting molecules, i.e., their conformation. The orientation of the eosin transition dipoles within its atomic structure was indicated by fluorescence polarization from oriented and immobilized dye in a stretched film [56]. The emission dipole was found to be parallel to the long axis of the xanthene ring. We assume this orientation for the emission dipole of all of the monomeric xanthene dyes used in our studies. The orientation of the xanthene absorption dipoles are surmised from the fluorescence excitation anisotropy of the randomly oriented and immobilized chromophore with the assumption that all of the dipoles lie in the plane of the xanthene ring. Then the ith dipole anisotropy, r_i, gives the angle in the plane, θ_i, between the absorption and emission dipole such that,

$$\cos^2\theta_i = \frac{5r_i + 1}{3} \tag{13}$$

If the xanthene plane is bisected into two half planes by the emission dipole vector then Eq. 13 contains no information about which half plane contains the ith absorption dipole. The angles θ_i and $\pi - \theta_i$ are also indistinguishable. We can choose among these four possibilities for the orientation of the ith absorption dipole based on how well the overall solution to the problem, made from particular choices for dipole orientation, accounts for the spectroscopic data (and NMR data in the case of rhodamine dimers, see reference [31]). The best solution for the conformation of the interacting molecules gives the orientation of all of the transition dipole moments including the emission dipole of the complex as described below in Section 3.5.

Several investigators using experimental or theoretical methods estimated the orientation of the lowest energy transition dipoles of indole, from the $^1A \rightarrow {}^1L_a$ and $^1A \rightarrow {}^1L_b$ transitions, within its atomic structure [41,42,57–60]. The orientation of two higher energy transition dipoles, from the $^1A \rightarrow {}^1B_a$ and $^1A \rightarrow {}^1B_b$ transitions, was estimated using semi-empirical calculations [41,42]. We assumed all dipoles lie within the plane of the indole ring. The dipole orientations of the $^1A \rightarrow {}^1B_a$ and $^1A \rightarrow {}^1B_b$ transitions were not confirmed experimentally, however, because of the large energy separation they couple weakly to the xanthene transitions under consideration here making our calculation relatively insensitive to their precise orientation.

3.5. The orientation of the emission dipole of a molecular complex

Polarized emission from a probe modified protein in a biological assembly reports the probe absorption and emission dipole orientation. If we know the relationship between the probe and the PHF then polarized emission intensities can be interpreted in terms of protein orientation. The latter possibility is why to study the tryptophan–probe geometry in S1, i.e., to determine the orientation of the probe in the PHF of the S1. Changes in the polarized emission signal from labeled fibers are then interpreted in terms of the motion of the S1 during muscle contraction.

The coupled dipole theory outlined in Section 3.2 provides the orientation and strength of the absorption dipoles of complexed molecules. The emission dipole vector of the complexed molecules is not given directly by this calculation but it is surmised by the following method. We assume that light emission from a molecular complex always occurs from the lowest energy excited state singlet. Then the observed anisotropy from the ith excited state of the complex, r_i, and Eq. 13 specifies a cone centered on the ith absorption dipole moment, μ_i, that contains the emission dipole on its surface. When μ_i and r_i are known for three distinct transitions their line of intersection gives the direction of the emission dipole. When μ_i and r_i are known for more than three transitions a nonlinear least squares method makes the best choice for the emission dipole orientation.

3.6. Energy transfer from S1 to a xanthene probe

Förster used the coupled dipole theory to calculate the rate of energy transfer between weakly coupled donor and acceptor chromophores [37]. Weak coupling implies that the extinction coefficients of the chromophores are not significantly perturbed by their interaction, or, as Förster states the criteria, $|U| < \Delta W$, where $|U|$ is the energy shift and ΔW is the width of the electronic transition. In the probe labeling of S1 we detect the probe but not the donor extinction coefficient because the donor is not uniquely identified. We find that the 5′IAF and the 5′IATR dimer absorption bands around 350 nm undergo a 5–13 nm red shift upon binding to S1 (see Table 1 Part II). This probe absorption band has the largest overlap with the emission from aromatic residues in S1. The energy shifts are considerably smaller that the width of the transition band so Förster theory is applicable although other transfer mechanisms may contribute.

We consider the possibility of Förster energy transfer between an aromatic residue of S1 (donor) and 5′IAF or 5′IATR dimer (acceptor) at SH1. The efficiency of transfer, $\Im$, is given by,

$$\Im = 1 - \frac{\epsilon_D F_{DA}}{\epsilon_{DA} F_D} = \frac{R_0^6}{R_0^6 + d^6} \qquad (14)$$

where ϵ_D (ϵ_{DA}) is the extinction coefficient of the donor in the absence (presence) of the acceptor, F_D (F_{DA}) is the emission intensity of the donor in the absence (presence) of the acceptor, R_0 is the characteristic energy transfer distance, and d is the distance from donor to acceptor [61]. We include the extinction coefficient of the donor in this formula to allow for the possibility of donor hyper/hypochromism due to the dipole–dipole coupling of the donor and acceptor. Quantities are expressed in terms of donor emission because, for protein–xanthene transfer, it is impossible to separate acceptor emission due to direct excitation from that due to energy transfer.

We estimate R_0 for 5′IATR and 5′IAF using,

$$R_0 = 9.79 \times 10^3 \left(\boldsymbol{K}^2 n^{-4} \phi_D J \right)^{1/6} \text{Å} \qquad (15)$$

where $\boldsymbol{K}^2$ is the orientation factor that we can calculate from our knowledge of the orientation of the donor emission and acceptor absorption dipoles, n is the index of refraction of water, ϕ_D is the quantum efficiency of the donor in the absence of the acceptor, and J is an integral related to the overlap of the acceptor extinction coefficient with the normalized donor fluorescence quantum spectrum. We calculated R_0 for tryptophan in S1 using $\phi_D = 0.20$ [62]. The donor emission spectral shape was measured from unlabeled S1 excited with light of wavelengths above 295 nm. S1 contains 5 tryptophans so that this shape is a weighted average of their emission [63]. The acceptor extinction coefficient should be estimated for the bound probe in the absence of the donor for the calculation of J. This condition is unachievable so we improvise by substituting the 5′IATR dimer or 5′IAF extinction coefficient in protein buffer. We found that $J = 0.18 \times 10^{-13}$ or 0.17×10^{-13} cm^3/M for tryptophan-5′IATR dimer or tryptophan-5′IAF pair. If $K^2 = 2/3$ then $R_0 \approx 25$ Å for both probes.

3.7. Probe orientation in the PHF of S1

We estimated the orientation of the lowest energy absorption and emission dipoles of the rhodamine dimer probe in the PHF of S1 using our method based on the analysis of data from multiple probes [4,5]. There we defined a coordinate frame, the dipole frame, where the emission dipole points along the z-axis and the absorption dipole falls in the first quadrant of the xz-plane. The dipole frame of 5′R-S1 relates to the PHF of S1 with Euler angles, $\Omega = (\alpha,\beta,\gamma)$. We showed that our multiple probe data is consistent with the two sets of Euler angles $\Omega_1 = (190°,60°,300°)$ or $\Omega_2 = (190°,120°,60°)$ were these angles specify the coordinate rotation from the principal to the dipole frame. In this calculation the shape of S1 was assumed to be an ellipsoid of revolution so that the choice $\alpha = 190°$ was arbitrary. In the present calculation the value of α is available as an adjustable parameter when fitting the probe to the SH1 binding pocket.

The α-carbon structure of S1 provides the information for calculating the orientation of its PHF [6]. Favro showed that, under the usual assumptions for rotational Brownian motion, elements of the rotational diffusion tensor, $D_{i,j}$, relate to elements of the viscous drag tensor, $\beta_{i,j}$, by Einstein's relation,

$$D_{i,j} = 1/2kT\left(\beta_{i,j}^{-1} + \beta_{j,i}^{-1} \right) \qquad (16)$$

where k is Boltzman's constant and T is temperature [64]. Our task is to estimate β using the positions of the α-carbons.

We attempted to estimate β, using methods for calculating the drag tensor for multisubunit structures with nonidentical subunits [65–70], with the amino acid residues centered on the α-carbon positions as the nonidentical subunits. In Appendix B we outline the derivation of β and the computation of the rotational diffusion tensor of S1 for a rigid S1 structure.

We obtained the PHF of S1 from the eigenvectors of the diffusion tensor. We determined the orientation of the lowest energy absorption and emission dipoles of the 5′IATR dimer relative to the dimer atomic structure, by the coupled oscillator method outlined above, and using the Euler angles relating the principal and dipole fixed frames (Ω_1 and Ω_2) we oriented the dimer in the SH1 binding pocket. We have not calculated the Euler angles relating the transition dipoles of fluorescein to the PHF of S1 when 5′IAF modifies S1. 5′IAF modified fibers gave fluorescence polarization ratios similar to those obtained with 5′IATR so we assume they are identical for the purposes of this calculation [71].

4. Experimental results

4.1. The Stokes shift from fluorescein and 5′F-S1

We investigated the Stokes wavelength shift, $\Delta\lambda_s$, from free 5′IAF and 5′F − S1 both in protein buffer as a function of temperature, and from fluorescein in the solvents acetonitrile, DMSO, ethanol, and acetone. The Stokes wavelength shifts are summarized in Table 1. There it is indicated that $\Delta\lambda_s$ for 5′F-S1 is identical to 5′IAF in protein buffer to within experimental error at the three temperatures investigated. The Stokes shifts in other solvents show a variability due to solvent polarity and refractive index.

4.2. Chiral amine induced CD in fluorescein

Fig. 2a and b show the absorption and CD spectrum from (*R*)-(+)-DMBA in acetonitrile. These spectra, characteristic of all three of the aromatic chiral amines investigated. i.e., DMBA, MBA, and DMPA, show a lowest energy transition at ca. 260 nm and a dipole strength ca. 1/100 the size of indole or tryptophan under similar conditions. The CD signals from the (*R*)- and (*S*)-chiral amines are opposite in sign. The aliphatic chiral amine ((*R*)-(+) and (*S*)-(−)-BA) absorbed light at higher energies. We investigated the effect of these chiral amines on the absorption and CD spectra from fluorescein as a model of the tryptophan–probe interaction in S1.

Concentrated fluorescein dissolved in DMF was added to acetonitrile and a large excess of the chiral amine. Fig. 3 shows the extinction coefficient of the fluorescein alone and with several concentrations of (*R*)-(+) − DMBA. The absorption spectrum shows a noticeable blue shift and a large decrease in dipole strength as the DMBA to fluorescein ratio increases. The dipole strength of fluorescein decreases ca. 30% in the presence of 1.5 M DMBA. DMBA binding to fluorescein can cause hypochromicity in fluorescein by the coupled dipole mechanism but the small dipole strength of the DMBA cannot induce the size

Table 1
Stokes wavelength shifts of 5′IAF in various solvents [a]

	5′F-S1	Buffer	DMSO	Acetonitrile	Ethanol	Acetone
d	–	78	47	37.5	25	20.7
n	–	1.33	1.478	1.344	1.328	1.359
$\Delta\lambda_s$ (T = 2°C)	18 ± 2	19 ± 2	–	–	–	–
$\Delta\lambda_s$ (T = 10°C)	17 ± 2	19 ± 2	–	–	–	–
$\Delta\lambda_s$ (T = 20°C)	19 ± 2	20 ± 2	17 ± 2	23 ± 2	14 ± 2	13 ± 2

[a] Listed are the dielectric constant, d, the refractive index, n, and the Stokes wavelength shift, $\Delta\lambda_s$, in nm (d and n are from CRC Handbook of Chemistry and Physics, 72nd edition). The Stokes wavelength shift of 5′F-S1 is identical to that of the free dye in protein buffer over the temperature range of 2–20°C.

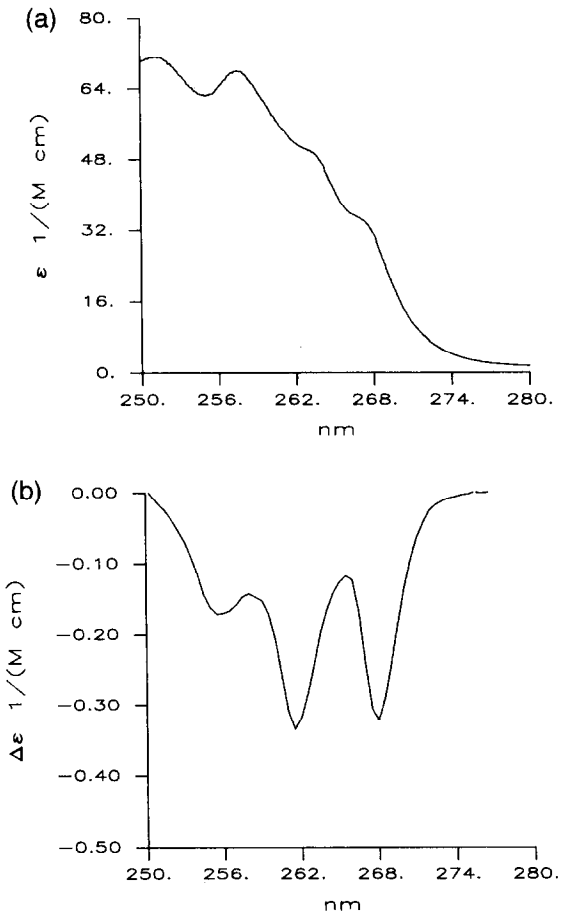

Fig. 2. The extinction coefficients from absorption (a) and CD (b) spectra of (*R*)-(+)-N,α-dimethylbenzylamine in acetonitrile.

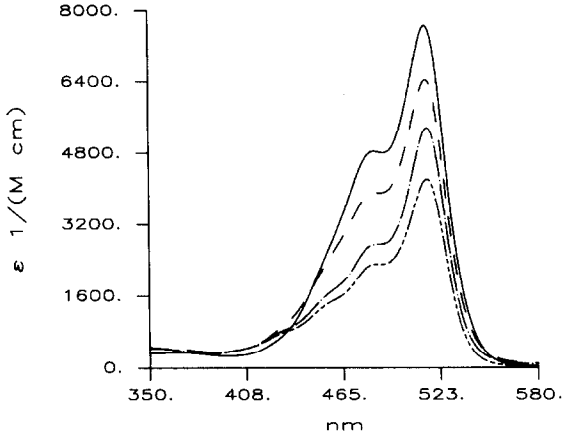

Fig. 3. The extinction coefficient of fluorescein as a function of concentration of the chiral amine (*R*)-(+)-DMBA. The four curves correspond to 150 μM fluorescein in the presence of 0 (—), 0.5 (- -), 1.0 (-·-), and 1.5 M (-· ·) concentration of chiral amine.

of change observed. The pH dependence of the fluorescein absorption spectrum shows that the protonated form of the probe is blue shifted and has a smaller dipole strength relative to the deprotonated form suggesting that the chiral amine induces protonation of the xanthene anion [72]. This apparent protonation of the fluorescein occurred with all of the aromatic amines but not with the aliphatic amine.

Fig. 4 shows the CD extinction coefficient spectrum from (*R*)-(+)- and (*S*)-(−)-DMBA interacting with fluorescein. Fluorescein has no CD signal under identical conditions but in the absence of DMBA. Both chiral amines induce a large CD signal that changes sign at ca. 470 nm wavelength suggesting the presence of two fluorescein species probably corresponding to the protonated (blue) and deprotonated (red) forms. The overall sign of the CD signal depends on the sign of the chirality of the DMBA. DMBA is most effective at inducing the CD signal in fluorescein, MBA is slightly less effective, while DMPA and BA do not induce a CD signal in fluorescein. The strength of the CD signal appears to depend on the basicity of the aromatic amine.

We attempted a semi-quantitative description of the chiral amine–probe complex based on the coupled dipole mechanism. We estimated the electric dipole strengths of the uncomplexed DMBA and

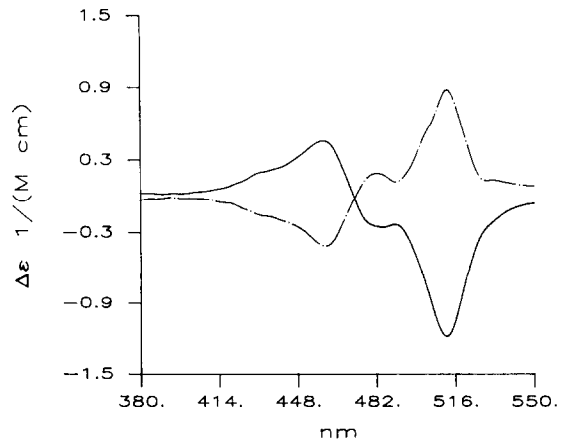

Fig. 4. The CD extinction coefficient of fluorescein with (*R*)-(+)-DMBA (—) and (*S*)-(−)-DMBA (-·-).

fluorescein from their absorption spectra, appearing in Figs. 2 and 3, and employing Eq. 7. We estimated a lower limit for the magnitude of the magnetic dipole moment of DMBA from the rotary strength, computed from the CD extinction coefficient of DMBA in Fig. 2 and employing Eq. 8, with the assumption that the magnetic and electric dipole moments are parallel (for (*S*)-(−)) or antiparallel (for (*R*)-(+)). We did not attempt to compare the observed dipole strength or peak absorption energy of the complex with that computed for the coupled dipole oscillators because the changes in the absorption spectrum of the complex from that of the free probe appears to be dominated by the shifts in the protonated–deprotonated fluorescein equilibrium. We did compare the observed rotary strength of the complex with that calculated for coupled dipole oscillators. We found that we could fully account for the observed rotary strength with the coupled dipole mechanism. The calculation suggests that the rotary strength of the complex could originate from the coupling mechanism involving chiral amine and probe dipoles.

It was suggested previously that an induced CD signal from a fluorescent probe could be caused by the stabilization of a particular asymmetrical conformation of constituent groups of the probe [10,32]. In our chiral amine–fluorescein system we might consider an asymmetrical conformation of the benzene and xanthene groups induced by the presence of the chiral amine. This stable conformation causes the coupling of the electric dipoles in these two constituent groups of fluorescein to give a CD signal. We explored this possibility by calculating the induced CD signal for coupled electric dipole oscillators originating from the xanthene and the benzene groups of fluorescein. We found this calculated rotary strength to be at least two orders of magnitude smaller than that observed for the chiral amine–fluorescein system indicating that the chiral amine induced CD signal is from the interaction of the intrinsic amine magnetic dipole with the xanthene electric dipoles. Induced CD was observed with similar strengths from fluorescein or hydroxyxantheneone (fluorescein without the benzene ring) bound to anti-fluorescein antibody indicating that induced chirality in fluorescein is independent of the intramolecular fluorescein conformation [15].

5. Discussion

The spectroscopic signal, originating from a specific and rigid probe of S1, contains a blend of local and global information about S1 internal structure and overall orientation. The implications of the signal for internal structure relates to the local environment on many levels. We have addressed here methods for the interpretation of the signals in terms of the probe–protein conformation based on the knowledge of the crystallographic structure of S1 [6].

The probe originating spectroscopic signals are perturbed by the local residues in the probe binding pocket. We quantitate these perturbations by comparing absorption, CD, and, fluorescence intensity and anisotropy of the probes in the presence and absence of the perturbants. We relate these spectroscopic parameters to the conformation of the probe itself, as in the study of dimer formation, and, to the distance and orientation of the probe relative to polarizable and/or polar perturbants, such as an aromatic side chain in a binding pocket, using coupled dipole and/or energy transfer models. Comparison of spectroscopic parameters that change upon the binding of a probe to a protein requires the identification of potential residues that can cause the observed perturbations. Our discussion of the effects probe–solvent interactions have on the spectroscopic parameters pointed out the difficulties in correctly identifying the residue. Thus we are obliged to seek additional guidance from independent experimental investigations two of which were identified here.

First, we described a model system for the probe–S1 interaction based on a chiral amine–fluorescent probe complex. This idea was based on earlier studies of the stereo chemical structure of bilirubin [9,73]. We wished to verify that a group possessing a magnetic dipole, like tryptophan, can induce a CD signal in the visible absorbance band of a probe like fluorescein. We found conditions where aromatic chiral amines induced CD in the lowest energy transition band of fluorescein. We found that we could fully account for the observed rotary strength of the complex with the coupled dipole mechanism and that all of the rotary strength of the complex originates from the coupling mechanism involving the intrinsic chiral amine magnetic dipole and the probe electric dipole. The aromatic chiral amine–fluorescent probe

model system demonstrates the feasibility of an aromatic residue induced CD signal from fluorescein or rhodamine bound to S1.

Second, we adapted here previously developed methods for computing the PHF of S1 based on the α-carbon structure of S1. Our computation of the PHF of S1 accounted for the rotational diffusion constants observed for S1 from the simultaneous analysis of X- and Q-band electron paramagnetic resonance (EPR) from spin labeled S1 in solution [4,5]. We will use the independently obtained information on the orientation of rhodamine or fluorescein absorption and emission dipoles within the PHF of S1 to help position the probe in the crystallographic structure of S1. The probe orientation information was obtained from measurements on probe modified muscle fibers in various physiological states. We will use the chiral amine model system, the orientation of the PHF of S1 relative to the probe absorption and emission dipoles, and the results of the coupled dipole oscillator modeling of the spectroscopic signals from the probe–S1 complex to help identify the conformation of the probe–S1 complex in Part II.

The atomic resolution description of probe–S1 conformation could prove to be valuable in the description of the intramolecular conformational changes in S1 accompanying hydrolysis of the enzyme substrate ATP during the production of force in muscle contractions. Other probes of SH1 and of other probe binding sites on myosin will provide interesting challenges for the future application of these methods to important question on the molecular mechanism of muscle contraction.

Acknowledgements

We gratefully acknowledge Daniel J. Toft for several experimental and conceptual contributions, and, Dr. Sungjo Park for critically reading the manuscript. Drs. P. Ilich, E. Klimtchuck, and S. Venyaminov made some preliminary measurements for this study. This work was supported by the National Institutes of Health grant R01 AR 39288, the American Heart Association Grant-in-Aid 930 06610, and the Mayo Foundation.

Appendix A. The bimolecular reaction in heterodimer formation

A mixture of two molecules, M_A and M_B, in solution may self-associate or associate with each other to form homodimers, heterodimers, or higher order complexes. Neglecting the higher order complexes the mixture forms homodimers, D_A and D_B, according to Eq. 1 and heterodimers, D_{AB}, such that,

$$M_A + M_B \underset{k_{2AB}}{\overset{k_{1AB}}{\rightleftarrows}} D_{AB} \tag{A1}$$

The equilibrium constants for this coupled system are, $K_A = k_{1A}/k_{2A}$, $K_B = k_{1B}/k_{2B}$, and $K_{AB} = k_{1AB}/k_{2AB}$. The equilibrium concentrations are the solutions to the coupled equations,

$$[M_{A0}] = [M_A] + 2K_A[M_A]^2 + K_{AB}[M_A][M_B] \tag{A2}$$

$$[M_{B0}] = [M_B] + 2K_B[M_B]^2 + K_{AB}[M_A][M_B]$$

Where we made use of the conservation of molecules requiring that $[M_{A0}] = [M_A] + 2[D_A] + [D_{AB}]$ and $[M_{B0}] = [M_B] + 2[D_B] + [D_{AB}]$. Equation A2 may be rewritten as a single quartic equation in $[M_A]$ (or M_B) and solved. The other equilibrium concentrations follow directly from the equilibrium constants.

The absorption, $A(\epsilon_{AB}; K_{AB})$, is linear in the extinction coefficients ϵ_{AB} for the heterodimer and nonlinear in K_{AB}. We measure A as a function of wavelength and at three or more $[M_{A0}]$'s or $[M_{B0}]$'s to obtain a column of points,

$$\begin{aligned} A_i = \Big\{ & \epsilon_A([D_A]_i/K_A)^{1/2} + \epsilon_{AA}[D_A]_i \\ & + \epsilon_B([D_B]_i/K_B)^{1/2} + \epsilon_{BB}[D_B]_i \\ & + \epsilon_{AB}[D_{AB}]_i \Big\} \ell_i \end{aligned} \tag{A3}$$

where subscript i refers to experiments with different initial dye concentrations and light paths, and subscripts on the extinction coefficients refer to monomers (A or B) or dimers (AA, BB, or AB). All parameters in Eq. A3 except for ϵ_{AB} and K_{AB} are known from homodimer experiments. For a particular choice of K_{AB} and wavelength, the unknown ϵ_{AB} in the set of Eqs. A3 is solved for by a least squares protocol with the constraint $\epsilon_{AB} \geq 0$. We found the

best choice for K_{AB} by the method described for homodimers in Section 3.1. The solution specifies a unique K_{AB} and ϵ_{AB} as a function of wavelength.

Appendix B. The viscous drag and diffusion tensors of myosin S1

The force vector, $\boldsymbol{F}_\ell$, on subunit ℓ moving with velocity vector $\boldsymbol{u}_\ell$ exerted by solvent flowing with velocity vector $\boldsymbol{v}_\ell$ is,

$$\boldsymbol{F}_\ell = \xi_\ell(\boldsymbol{v}_\ell - \boldsymbol{u}_\ell) \tag{B1}$$

where ξ_ℓ is the frictional coefficient of subunit ℓ. Solvent velocity, $\boldsymbol{v}_\ell$, is the solvent flow in the absence of the solute, $\boldsymbol{v}^0$, plus a perturbation caused by the presence of solute, $\boldsymbol{v}$, such that $\boldsymbol{v}_\ell = \boldsymbol{v}^0 + \boldsymbol{v}'_\ell$. The solvent flow velocity in the absence of solute does not depend on position so that the ℓ subscript is dropped. The perturbation is given by,

$$\boldsymbol{v}'_\ell = -\sum_{\substack{s=1 \\ s\neq\ell}}^{n} T_{\ell,s}\boldsymbol{F}_s \tag{B2}$$

where n is the number of residues and $T_{\ell,s}$ is the modified Oseen tensor appropriate for nonidentical subunits [70]. The subunit velocity viewed from a coordinate frame fixed in space is from both translational and rotational movement so that [74],

$$\boldsymbol{u}_\ell = \boldsymbol{u}^0 + \omega \times \boldsymbol{r}_\ell \tag{B3}$$

where $\boldsymbol{u}^0$ is the center of mass velocity of the protein that is the same for all subunits, ω is the angular velocity vector of the S1, and $\boldsymbol{r}_\ell$ is the vector joining the center of mass with subunit ℓ. Substituting the lowest order approximation,

$$\boldsymbol{F}_s = \xi_s(\boldsymbol{v}^0 - \boldsymbol{u}_s) \tag{B4}$$

into Eq. B1 and then using Eqs. B2 and B3 we obtain,

$$\boldsymbol{F}^0_\ell = \xi_\ell\left(\mathbb{I} - \sum_{s\neq\ell}^{n}\xi_s T_{\ell,s}\right)(\boldsymbol{v}^0 - \boldsymbol{u}^0) + \xi_\ell\left(-\omega\times\boldsymbol{r}_\ell + \sum_{s\neq\ell}^{n}\xi_s T_{\ell,s}\omega\times\boldsymbol{r}_\ell\right) \tag{B5}$$

The superscript on $\boldsymbol{F}^0_\ell$ refers to the order of the approximation. The next order of approximation would be obtained by replacing Eq. B4 with B5 and substituting into Eq. B1. Higher order approximations are obtained similarly. The first term in Eq. B5, related to translational diffusion, is ignored subsequently. The torque on subunit ℓ is $\boldsymbol{r}_\ell \times \boldsymbol{F}^i_\ell$ so that to lowest order the total torque on the protein due to the viscous drag of the solvent, $\boldsymbol{N}$, is,

$$\boldsymbol{N} = \sum_{\ell=1}^{n}\xi_\ell\boldsymbol{r}_\ell \times \left(-\omega\times\boldsymbol{r}_\ell + \sum_{s\neq\ell}^{n}\xi_s T_{\ell,s}\omega\times\boldsymbol{r}_\ell\right) \tag{B6}$$

Carrying out the cross products, Eq. B6 can be rewritten as,

$$\boldsymbol{N} = \sum_{\ell=1}^{n}\xi_\ell\left(-I_\ell/m_\ell + \sum_{s\neq\ell}^{n}\xi_s G^i_{\ell,s}\right)\omega \tag{B7}$$

where I_ℓ is the moment of inertia tensor and m_ℓ the mass of the ℓth subunit and tensor $G^i_{\ell,s}$ depends only on the distribution and modified Oseen tensor of the subunits. Eq. B7 is correct for the ith order of approximation of $\boldsymbol{F}^i_\ell$ with G suitably modified. Comparing the Langevin equation with Eq. B7 (64) implies that the viscous drag tensor for the ith order approximation, β^i, is given by,

$$\beta^i = \sum_{\ell=1}^{n}\xi_\ell\left(I_\ell/m_\ell - \sum_{s\neq\ell}^{n}\xi_s G^i_{\ell,s}\right) \tag{B8}$$

Stokes Law with stick boundary conditions says that the friction coefficient $\xi_\ell = 6\pi\eta R_\ell$ for spherical subunits of Stokes radius R_ℓ and solvent viscosity η. Assuming that myosin's mass is uniformly distributed within its hydrated volume, $R_\ell = (3V_2 m_\ell/4\pi)^{1/3}$, where $V_2 \approx 1.08$ cm^3/g is the specific volume of hydrated myosin, we obtained Stokes radii for the amino acid residues ranging from 3–4 Å. We obtained best results for R_ℓ renormalized to range from 2–3 Å and when only every third residue of the 1072 residues in the α-carbon structure is included in the summation over subunits in Eq. B8.

We used an expression for tensor $G_{\ell,s}$ in Eq. B7 consistent with including up to 2nd order terms in the approximation for $\boldsymbol{F}_s$. When computing the contribution from terms containing the modified Oseen interaction tensor we found it necessary to limit the sum over interacting subunits to those nearest neighbors within a distance of 6 Stokes radii. Without this

weighting of subunit interactions, the many small contributions from distant residues in the protein overwhelmed the more important contributions from the nearest neighbor residues. Using a solvent viscosity appropriate for water at 5°C, $\eta \approx 1550$ μPa s, we computed the viscous drag tensor and used Eq. 16 to find the diffusion tensor. The diagonalized diffusion tensor is $D_{x,x} = 2.1 \times 10^5$ s^{-1}, $D_{y,y} = 2.3 \times 10^5$ s^{-1}, and $D_{z,z} = 1.0 \times 10^6$ s^{-1} in good agreement with our experimentally measured values of $D_{x,x} = D_{y,y} = 2.2 \times 10^5$ s^{-1} and $D_{z,z} = 1.0 \times 10^6$ s^{-1} [5].

References

[1] J. Borejdo, S. Putnam and M.F. Morales, Proc. Natl. Acad. Sci. USA, 76 (1979) 6346–6350.
[2] J. Borejdo, O. Assulin, T. Ando and S. Putnam, J. Mol. Biol., 158 (1982) 391–414.
[3] E.H. Hellen, K. Ajtai and T.P. Burghardt, J. Fluoresc., 5 (1995) 355–367.
[4] T.P. Burghardt and K. Ajtai, Biochemistry, 33 (1994) 5376–5381.
[5] K. Ajtai, D.J. Toft and T.P. Burghardt, Biochemistry, 33 (1994) 5382–5391.
[6] I. Rayment, W.R. Rypniewski, K. Schmidt-Bäse, R. Smith, D.R. Tomchick, M.M. Benning, D.A. Winkelman, G. Wesenberg and H.M. Holden, Science, 261 (1993) 50–58.
[7] I. Tinoco, J. Chem. Phys., 33 (1960) 1332–1338.
[8] I. Tinoco, J. Chem. Phys., 34 (1961) 1067.
[9] D.H. Lightner, J.-Y. An and Y.-M. Pu, Arch. Biochem. Biophys., 262 (1988) 543–559.
[10] J.F. Towell and R.W. Woody, Biochemistry, 19 (1980) 4231–4237.
[11] R.A. Edwards and R.W. Woody (1977), Biochem. Biophys. Res. Commun., 79, 470–476.
[12] R.A. Edwards and R.W. Woody, Biochemistry, 18 (1979) 5197–5204.
[13] R.A. Edwards and R.W. Woody, J. Phys. Chem., 87 (1983) 1329–1337.
[14] J.R. Gollogly and R.E. Cathou, J. Immunol., 113 (1974) 1457–1467.
[15] T.W. Athey and R.E. Cathou, Immunochemistry, 14 (1977) 397–404.
[16] S.Y. Tetin, W.W. Mantulin, L.K. Denzin, K.M. Weidner and E.W. Voss, Biochemistry, 31 (1992) 12029–12034.
[17] C.G. dos Remedios, M. Miki and J.A. Barden, J. Muscle Res. Cell Motility, 8 (1985) 97–117.
[18] E.E. Huston, J.C. Grammer and R.G. Yount, Biochemistry, 27 (1988) 8945–8952.
[19] J. Botts, J.F. Thomason and M.F. Morales, Proc. Natl. Acad. Sci. USA, 86 (1989) 2204–2208.
[20] R. Aguirre, S.-H. Lin, F. Gonsoulin, C.-K. Wang and H.C. Cheung, Biochemistry, 28 (1989) 799–807.
[21] R. Agarwal, K.N. Rajasekharan and M. Burke, J. Biol. Chem., 226 (1991) 2272–2275.
[22] T. Hiratsuka, J. Biol. Chem., 267 (1992) 14941–14948.
[23] T. Hiratsuka, J. Biol. Chem., 267 (1992) 14949–14954.
[24] T. Hiratsuka, J. Biol. Chem., 268 (1993) 24742–24750.
[25] T. Hiratsuka, J. Biol. Chem., 269 (1994) 27251–27257.
[26] R.G. Yount, C.R. Cremo, J.C. Grammer and B.A. Kerwin, Phil. Trans. R. Soc. London B, 336 (1992) 55–61.
[27] B.C. Phan, P. Cheung, C.J. Miller, E. Reisler and A. Muhlrad, Biochemistry, 33 (1994) 11286–11295.
[28] K. Ajtai and T.P. Burghardt, Biochemistry, 34 (1995) 15943–15952.
[29] K. Ajtai, P.J.K. Ilich, A. Ringler, S.S. Sedarous, D.J. Toft and T.P. Burghardt, Biochemistry, 31 (1992) 12431–12440.
[30] T.P. Burghardt, J.E. Lyke and K. Ajtai, Biophys. Chem., 59 (1996) 119–131.
[31] P. Ilich, P. Mishra, S. Macura and T.P. Burghardt, Spectrochim. Acta A, (1996) in press.
[32] J.S. Wicken and R.W. Woody, Biochemistry, 12 (1973) 3459–3466.
[33] R.S. Cahn, C.K. Ingold and V. Prelog, Experientia, 12 (1956) 81.
[34] R.S. Cahn, C.K. Ingold and V. Prelog, Angew. Chem. Int. Ed. Engl., 5 (1966) 385.
[35] V. Prelog and G. Helmchem, Angew. Chem. Int. Ed. Engl., 21 (1982) 567.
[36] G. Strang, in Introduction to Applied Mathematics, 1986, Wellesley, MA, pp. 87–137.
[37] Th. Förster, in D. Sinanoĥlu (Ed.), Modern Quantum Chemistry, 1965, Academic Press, New York, pp. 93–137.
[38] R.W. Woody, J. Chem. Phys., 49 (1968) 4797–4806.
[39] M.-C. Hsu and R.W. Woody, J. Am. Chem. Soc., 93 (1971) 3515–3525.
[40] A.K. Chen and R.W. Woody, J. Am. Chem. Soc., 93 (1971) 29–37.
[41] W.J. Goux, T.R. Kadesch and T.M. Hooker, Jr., Biopolymers, 15 (1976) 977–997.
[42] P. Ilich and F.G. Prendergast, Biopolymers, 32 (1992) 667–694.
[43] P.M. Bayley, E.B. Nielsen and J.A. Schellman, J. Phys. Chem., 73 (1969) 228–243.
[44] J.A. Schellman, Chem. Rev., 75 (1975) 323–331.
[45] E.B. Nielsen and J.A. Schellman, J. Phys. Chem., 71 (1967) 2297–2304.
[46] J.A. Schellman and E.B. Nielsen, J. Phys. Chem., 71 (1967) 3914–3921.
[47] T.M. Hooker, Jr. and J.A. Schellman, Biopolymers, 9 (1970) 1319–1348.
[48] N.S. Bayliss, J. Chem. Phys., 18 (1950) 292–296.
[49] R.A. Marcus, J. Chem. Phys., 24 (1956) 979–989.
[50] R.A. Marcus, J. Chem. Phys., 38 (1963) 1858–1862.
[51] R.A. Marcus, J. Chem. Phys., 39 (1963) 460–469.
[52] R.A. Marcus, J. Chem. Phys., 43 (1965) 1261–1274.
[53] E.G. McRae, J. Phys. Chem., 61 (1957) 562–572.
[54] N.S. Bayliss and E.G. McRae, J. Phys. Chem., 58 (1954) 1002–1006.

[55] G. Weber and F.J. Farris, Biochemistry, 18 (1979) 3075–3078.
[56] U.A. van der Heide, B. Orbons, H.C. Gerritsen and Y.K. Levine, Eur. Biophys. J., 21 (1992) 263–272.
[57] C.-T. Chang, C.-Y. Wu, A.R. Muirhead and J.R. Lombardi, Photochem. Photobiol., 19 (1974) 347–351.
[58] B. Valeur and G. Weber, Photochem. Photobiol., 25 (1977) 441–444.
[59] L.A. Phillips and D.H. Levy, J. Chem. Phys., 85 (1986) 1327–1332.
[60] B. Albinsson, M. Kubista, B. Nordén and E.W. Thulstrup, J. Phys. Chem., 93 (1989) 6646–6654.
[61] J.R. Lakowicz, Principles of Fluorescence Spectroscopy, 1983, Plenum Press, New York, pp. 303–339.
[62] C.R. Cantor and P.R. Schimmel, Biophysical Chemistry Part II, 1980, Freeman, New York, pp. 409–480.
[63] P.M. Torgerson, Biochemistry, 23 (1984) 3002–3007.
[64] L.D. Favro, Physical Rev., 119 (1960) 53–62.
[65] J.G. Kirkwood, J. Polymer Sci., 12 (1954) 1–14.
[66] J. Riseman and J.G. Kirkwood, Rheology, Vol. 1, 1956, Academic Press, New York, pp. 495–523.
[67] J.E. Hearst and W.H. Stockmayer, J. Chem. Phys., 37 (1962) 1425–1433.
[68] J.E. Hearst, J. Chem. Phys., 38 (1963) 1062–1065.
[69] V. Bloomfield, W.O. Dalton and van K.E. Holde, Biopolymers, 5 (1967) 135–148.
[70] de la J.G. Torre and V.A. Bloomfield, Biopolymers, 16 (1977) 1765–1778.
[71] K. Ajtai and T.P. Burghardt, Biochemistry, 31 (1992) 4275–4288.
[72] M.M. Martin and L. Lindqvist, J. Luminesc., 10 (1975) 381–390.
[73] D.H. Lightner, J.K. Gawronski and W.M.D. Wijekoon, J. Am. Chem. Soc., 109 (1987) 6354–6362.
[74] H. Goldstein, Classical Mechanics, 1950, pp. 93–184.